Emergent Ergodicity at the Transition between Many-Body Localized Phases

Rahul Sahay [1,*] Francisco Machado [1,*] Bingtian Ye [1,*] Chris R. Laumann [2] and Norman Y. Yao [1,3]

[1]*Department of Physics, University of California, Berkeley, California 94720, USA*
[2]*Department of Physics, Boston University, Boston, Massachusetts 02215, USA*
[3]*Materials Science Division, Lawrence Berkeley National Laboratory, Berkeley, California 94720, USA*

Strongly disordered systems in the many-body localized (MBL) phase can exhibit ground state order in highly excited eigenstates. The interplay between localization, symmetry, and topology has led to the characterization of a broad landscape of MBL phases ranging from spin glasses and time crystals to symmetry protected topological phases. Understanding the nature of phase transitions between these different forms of eigenstate order remains an essential open question. Here, we conjecture that no direct transition between distinct MBL orders can occur in one dimension; rather, an ergodic phase always intervenes. Motivated by recent advances in Rydberg-atom-based quantum simulation, we propose an experimental protocol where the intervening ergodic phase can be diagnosed via the dynamics of local observables.

Traditionally, the classification of phases of matter has focused on systems at or near thermal equilibrium. Many-body localization (MBL) offers an alternative to this paradigm [1–6]. In particular, owing to the presence of strong disorder, MBL phases are characterized by their failure to thermalize [7–10]. This dynamical property imposes strong constraints on the structure of eigenstates; namely, that they exhibit area-law entanglement and can be described as the ground state of quasi-local Hamiltonians [11,12]. Perhaps the most striking consequence is that such systems can exhibit order—previously restricted to the ground state—throughout their entire many-body spectrum [12–17]. This offers a particularly tantalizing prospect for near-term quantum simulators: The ability to observe phenomena, such as coherent topological edge modes, without the need to cool to the many-body ground state [18–22].

The presence of eigenstate order in the many-body localized phase also raises a more fundamental question: What is the nature of phase transitions between different types of MBL order? This question highlights a delicate balance between the properties of localization and phase transitions. On the one hand, the stability of MBL is contingent upon the existence of an extensive number of quasilocal conserved quantities ("ℓ-bits") [11,23]. On the other hand, the correlation length at a second-order phase transition *diverges* [24]. Understanding and characterizing this interplay remains an outstanding challenge. Indeed, while certain studies suggest the presence of a direct transition between distinct MBL phases [16,20,25–28], others have found signatures of delocalization at the transition [29–31].

In this Letter, we conjecture that any transition between distinct MBL phases is invariably forbidden and that an

intervening ergodic phase always emerges [Fig. 1(a)]. This conjecture is motivated by an extensive numerical study of three classes of MBL transitions: (i) a symmetry-breaking transition, (ii) a symmetry-protected topological (SPT) transition, and (iii) a discrete time crystalline transition (in a Floquet system). By systematically constructing the various phase diagrams, we show that an intervening ergodic region emerges for all numerically accessible interaction strengths. Moreover, we demonstrate that this emergent ergodicity is intimately tied to the presence of a phase transition; a *disorderless*, symmetry-breaking field suppresses the intervening ergodic phase. In addition to
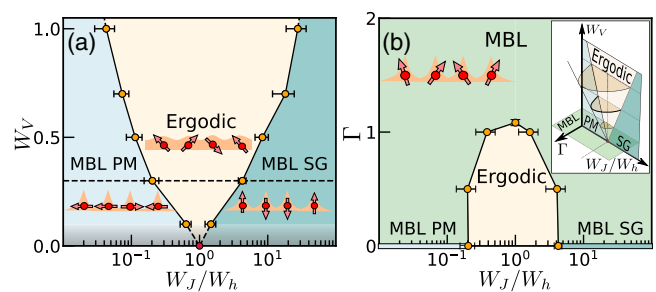

FIG. 1. (a) Phase diagram of the symmetry breaking model, Eq. (1), as a function of W_J/W_h and interaction strength W_V. For all numerically accessible W_V (outside the shaded region), we observe a finite width ergodic region between the two different MBL phases (PM and SG). At $W_V = 0$, the system is noninteracting and exhibits a critical point at $W_J/W_h = 1$ (red point). (b) Phase diagram as a function of a symmetry breaking field Γ and W_J/W_h for $W_V = 0.3$. With increasing Γ, the size of the ergodic region decreases until the system remains localized for all W_J/W_h. (inset) Schematic of the full phase diagram as a function of W_J/W_h, W_V and Γ.
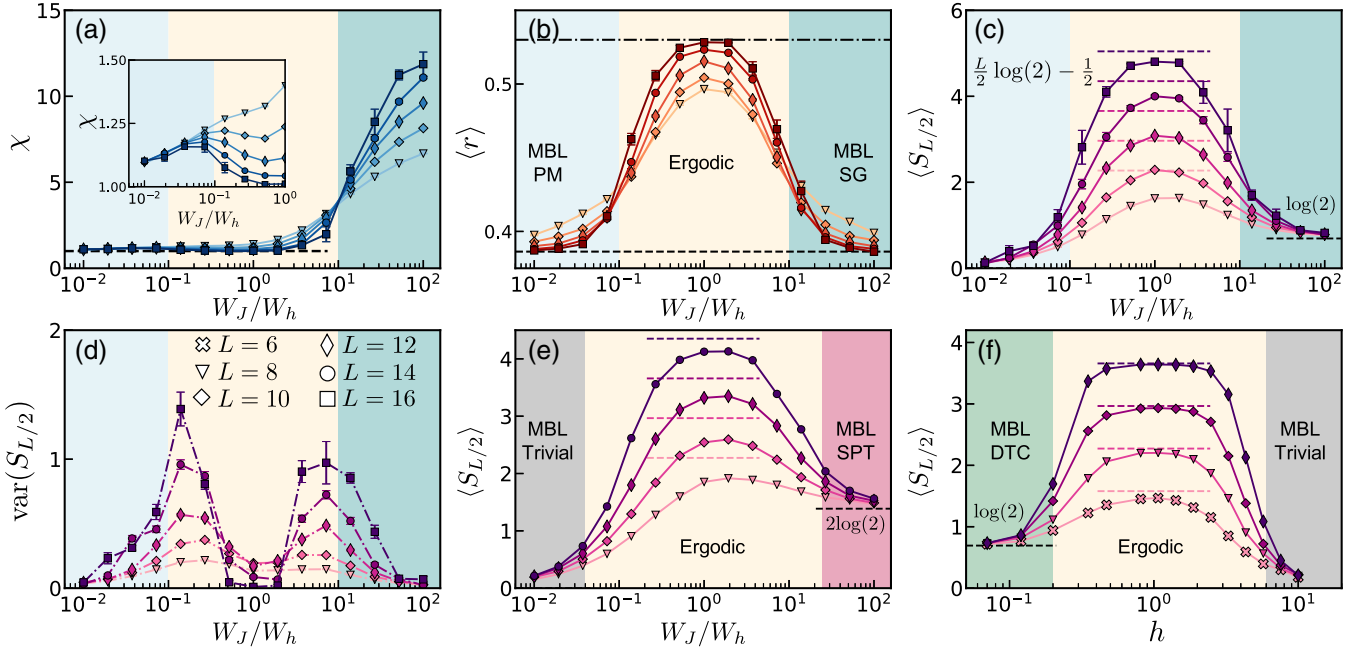
FIG. 2. (a)–(d) Characterization of the symmetry breaking model, Eq. (1), for $W_V = 0.7$. (a) For $W_J/W_h \gtrsim 10$, χ increases with system size evincing the SG nature of the phase. In the PM phase, χ approaches a finite constant, albeit exhibiting two distinct behaviors (inset). (b) $\langle r \rangle$-ratio as a function of W_J/W_h reveals an intervening ergodic phase surrounded by two localized phases. The dash-dotted [dashed] line corresponds to the GOE [Poisson] expectation. (c) The half-chain entanglement entropy $S_{L/2}$ increases with system size for intermediate W_J/W_h, in agreement with the expected thermal volume law. In the two localized phases, $S_{L/2}$ saturates to different values, highlighting the distinct nature of the underlying eigenstate order. (d) The variance of $S_{L/2}$ exhibits two distinct peaks in agreement with the presence of two distinct transitions. (e)[(f)] $S_{L/2}$ for the SPT [DTC] model of Eq. (2) [Eq. (3)] also demonstrates the presence of an intervening ergodic phase. Each data point corresponds to averaging over at least 10^3 disorder realizations.

numerics, we analyze two instabilities which could induce thermalization near the putative transition: (i) the proliferation of two-body resonances [2,32,33] and (ii) the run-away of "avalanches" [34,35]. We find that the latter is marginal. Finally, we propose and analyze an experimental platform capable of directly exploring the emergence of ergodicity at the transition between MBL phases. Our proposal is motivated by recent advances in Rydberg-dressed, neutral-atom quantum simulators [36–43]; we demonstrate that the phase diagram depicted in Fig. 1 can be directly probed via quench dynamics of local observables within experimental decoherence timescales.

Let us start by considering the paradigmatic example of a disordered one dimensional spin chain, which hosts two distinct MBL phases:

$$H = \sum_i J_i \sigma_i^z \sigma_{i+1}^z + \sum_i h_i \sigma_i^x + \sum_i V_i (\sigma_i^x \sigma_{i+1}^x + \sigma_i^z \sigma_{i+2}^z), \quad (1)$$

where $\vec{\sigma}$ are Pauli operators and all coupling strengths are disordered, with $J_i \in [-W_J, W_J]$, $h_i \in [-W_h, W_h]$, and $V_i \in [-W_V, W_V]$ [44]. We choose to work with the normalization $\sqrt{W_J W_h} = 1$ and perform extensive exact diagonalization studies up to system size $L = 16$ [45]. In the absence of V_i, the system reduces to the non-interacting, Anderson localized limit and for sufficiently

strong disorder (in J_i and h_i), this localization persists in the presence of interactions.

The Hamiltonian [Eq. (1)] exhibits a $\mathbb{Z}_2$ symmetry corresponding to a global spin flip, $G = \prod_i \sigma_i^x$. In the many-body localized regime, two distinct forms of eigenstate order emerge with respect to the breaking of this symmetry. For $W_h \gg W_J, W_V$, the transverse field dominates and the system is in the MBL paramagnetic (PM) phase. The conserved ℓ-bits simply correspond to dressed versions of the physical σ_i^x operators. For $W_J \gg W_h, W_V$, the Ising interaction dominates and the eigenstates correspond to "cat states" of spin configurations in the $\hat{z}$ direction. Physical states break the associated $\mathbb{Z}_2$ symmetry, the ℓ-bits are dressed versions of $\sigma_i^z \sigma_{i+1}^z$, and the system is in the so-called MBL spin-glass (SG) phase [13,16].

These two types of eigenstate order can be distinguished via the Edwards-Anderson order parameter which probes the presence of long-range Ising correlations in eigenstates $|n\rangle$, $\chi = \langle\!\langle L^{-1} \sum_{i,j} \langle n | \sigma_i^z \sigma_j^z | n \rangle^2 \rangle\!\rangle$, where $\langle\!\langle \cdots \rangle\!\rangle$ denotes averaging over disorder realizations [16,28]. In the SG phase, this order parameter scales extensively with system size, $\chi \propto L$, while in the PM phase, it approaches a constant $\mathcal{O}(1)$ value. Fixing $W_V = 0.7$, χ exhibits a clear transition from PM to SG as one tunes the ratio of W_J/W_h [Fig. 2(a)]. The finite-size flow of χ is consistent

with the presence of a *single* critical point at $W_J = 3.2$, $W_h = 0.32$ ($W_J/W_h \approx 10$).

However, thermalization diagnostics tell a different story. In particular, we compute the $\langle r \rangle$-ratio, a measure of the rigidity of the many-body spectrum: $\langle r \rangle = \langle\!\langle \min\{\delta_n, \delta_{n+1}\}/\max\{\delta_n, \delta_{n+1}\} \rangle\!\rangle$, where $\delta_n = E_{n+1} - E_n$, E_n is the nth eigenenergy and averaging is also done across the entire many-body spectrum [46,47]. In the MBL phase, energy levels exhibit Poisson statistics with $\langle r \rangle \approx 0.39$, while in the ergodic phase, level repulsion leads to the Gaussian Orthogonal Ensemble (GOE) expectation $\langle r \rangle \approx 0.53$ [4,6,8]. Unlike χ, which exhibits a single transition, the $\langle r \rangle$-ratio exhibits two distinct critical points, each characterized by its own finite-size flow [Fig. 2(b)]. This demarcates three distinct phases: two many-body localized phases (for $W_J/W_h \lesssim 0.1$ and $W_J/W_h \gtrsim 10$) separated by an intervening ergodic phase. Interestingly, the location of the ergodic-MBL transition at $W_J/W_h \approx 10$ matches the location of the spin-glass transition observed via χ. The fact that an additional ergodic-MBL transition is observed in the $\langle r \rangle$-ratio, but not in χ, suggests that the PM regime has slightly more structure.

In order to further probe this structure, we turn to the half-chain entanglement entropy, $S_{L/2} = -\text{Tr}[\rho_s \log(\rho_s)]$, where $\rho_s = \text{Tr}_{i \leq L/2}[|n\rangle\langle n|]$ [6,11,16,48–55]. The behavior of $S_{L/2}$, illustrated in Fig. 2(c), allows us to clearly distinguish three phases: the MBL paramagnet, the ergodic paramagnet, and the MBL spin glass. For $W_J/W_h \ll 0.1$, the eigenstates are close to product states and the entanglement entropy $S_{L/2}$ is independent of L, consistent with a localized paramagnet. Near $W_J/W_h \approx 1$, $S_{L/2}$ increases with system size, approaching $(L \log 2 - 1)/2$, consistent with an ergodic paramagnet [56]. Finally, for $W_J/W_h \gg 10$, the half-chain entanglement again becomes independent of L and, for very large W_J/W_h, approaches $\log 2$, consistent with the cat-state-nature of eigenstates in the MBL SG phase.

A few remarks are in order. First, the variance of $S_{L/2}$ across the ensemble of disorder realizations provides a complementary diagnostic to confirm the presence of two distinct ergodic-MBL transitions [Fig. 2(d)] [16,49–55]. Indeed, one observes two well-separated peaks in $\text{var}(S_{L/2})$, whose locations are consistent with the transitions found in the $\langle r \rangle$-ratio. Second, although χ only scales with system size in the SG phase, one expects its behavior to be qualitatively different in the MBL versus ergodic paramagnet. In particular, in the MBL paramagnet, the ℓ-bits have a small overlap with $\sigma_i^z \sigma_j^z$ and one expects $\chi > 1$; meanwhile, in the ergodic paramagnet, for a state chosen at the center of the many-body spectrum, one expects that $\chi \to 1$ rapidly with increasing system size (owing to the eigenstate thermalization hypothesis) [8,57–59]. This is indeed borne out by the numerics, as shown in the inset of Fig. 2(a).

Diagnostics in hand, we now construct the full phase diagram as a function of W_V and W_J/W_h [Fig. 1(a)]. Even
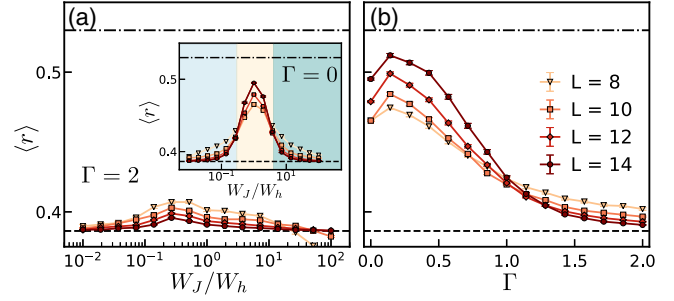

FIG. 3. (a) $\langle r \rangle$-ratio as a function of W_J/W_h at $W_V = 0.3$ in the presence of an explicit symmetry breaking field $\Gamma = 2$. The dash-dotted [dashed] line corresponds to the GOE [Poisson] expectation. Unlike the symmetry respecting case ($\Gamma = 0$, inset), the system remains localized for all values of W_J/W_h. (b) Within the ergodic region (here with $W_J/W_h = 1$), an increasing symmetry-breaking field drives the system towards localization. Each data point corresponds to averaging over at least 3×10^2 disorder realizations.

for the smallest interaction strengths accessible $W_V \sim 0.07$ (i.e., where the minimum interaction coupling remains larger than the mean level spacing) one observes a finite width region where the $\langle r \rangle$-ratio increases with system size [45,48,60,61]. Although clearly indicative of an ergodic intrusion, it is possible that our analysis underestimates the size of the intervening ergodic phase [48,62,63]. Extrapolating toward $W_V = 0$, our phase diagram suggests the presence of a finite-width thermal region between the two MBL phases, which terminates at the non-interacting critical point [Fig. 1(a)].

To verify that the presence of a phase transition is indeed responsible for the intervening ergodic region, one can explicitly break the $\mathbb{Z}_2$ symmetry in Eq. (1). We do so by adding a *disorderless*, on-site longitudinal field, $\Gamma \sum_i \sigma_i^z$. Despite the fact that the field is uniform, it causes the $\langle r \rangle$-ratio to systematically decrease [Figs. 3(a) and 3(b)], and for a sufficiently large symmetry breaking field, all finite-size flow tends toward localization. This allows us to construct the phase diagram in the presence of finite Γ, as depicted in Fig. 1(b) for $W_V = 0.3$.

To understand the generality of an emergent ergodic region between many-body localized phases, we now consider two additional types of MBL transitions: a symmetry-protected topological (SPT) transition and a discrete time-crystalline (DTC) transition. The Hamiltonian of the SPT model is given by [64]

$$H_{\text{SPT}} = \sum_i J_i \sigma_{i-1}^z \sigma_i^x \sigma_{i+1}^z + \sum_i h_i \sigma_i^x$$
$$+ \sum_i V_i (\sigma_i^x \sigma_{i+1}^x + \sigma_{i-1}^z \sigma_i^y \sigma_{i+1}^y \sigma_{i+2}^z), \quad (2)$$

with $J_i \in [-W_J, W_J]$, $h_i \in [-W_h, W_h]$, and $V_i \in [-W_V, W_V]$. H_{SPT} exhibits a $\mathbb{Z}_2 \times \mathbb{Z}_2$ symmetry, which gives rise to an MBL SPT (Haldane) phase for $W_J \gg W_h, W_V$ and a

topologically trivial MBL phase for $W_h \gg W_J, W_V$ [15,18,65]. For the DTC model, we consider the Floquet unitary evolution $U_F = \mathcal{T} \exp[-i \int_0^T H_F(t) dt]$ generated by the stroboscopic Hamiltonian:

$$H_F(t) = \begin{cases} \sum_i J_i \sigma_i^z \sigma_{i+1}^z + h_i \sigma_i^x + V_i \sigma_i^z & t \in [0, T/2] \\ -\frac{\pi}{T} \sum_i \sigma_i^x & t \in [T/2, T) \end{cases} \quad (3)$$

where $J_i \in [0.5, 1.5]$, $T = 2$, $h_i \in [0, h]$ and $V_i \in [0, 2V]$. When $h \ll 1$, the Floquet system spontaneously breaks time-translation symmetry and is in the so-called DTC phase, while for $h \gg 1$, the system is in a Floquet paramagnetic phase [20,21,29,66–68]. We analyze each of these models using the four diagnostics previously described: (i) the order parameter, (ii) the $\langle r \rangle$-ratio, (iii) the half-chain entanglement, and (iv) the variance, $\text{var}(S_{L/2})$. We observe the same qualitative behavior for both transitions across all diagnostics: An intervening ergodic phase emerges which terminates at the noninteracting critical point. This is illustrated in Figs. 2(e) and 2(f) using $S_{L/2}$ for both the SPT model (for an eigenstate of H_{SPT} at zero energy density) and the DTC model (for an eigenstate of U_F at π quasienergy); all additional data for the different diagnostics can be found in the Supplemental Material [45]. We further analyze the finite-size effects arising from small couplings [45], which we believe underlie previous numerical observations of apparent direct transitions [20,26–28].

Experimental realization.—Motivated by recent advances in the characterization and control of Rydberg states, we propose an experimental protocol to directly explore the emergence of ergodicity between MBL phases. Our protocol is most naturally implemented in one-dimensional chains of either alkali or alkaline-earth atoms [36–43]. To be specific, we consider ^{87}Rb with an effective spin-1/2 encoded in hyperfine states: $|\downarrow\rangle = |F = 1, m_F = -1\rangle$ and $|\uparrow\rangle = |F = 2, m_F = -2\rangle$. Recent experiments have demonstrated the ability to generate strong interactions via either Rydberg dressing in an optical lattice (where atoms are typically spaced by $\sim 0.5 \ \mu\text{m}$) or via Rydberg blockade in a tweezer array (where atoms are typically spaced by $\sim 3 \ \mu\text{m}$) [36–43]. Focusing on the optical lattice setup, dressing enables the generation of tunable, long-range soft-core Ising interactions, $H_{ZZ} = \sum_{i,j} J_{ij} \sigma_i^z \sigma_j^z$, with a spatial profile that interpolates between a constant at short distances (determined by the blockade radius) and a $1/r^6$ van der Waals tail.

A particularly simple implementation of a PM-SG Hamiltonian [closely related to Eq. (1)] is to alternate time evolution under H_{ZZ} and $H_X = \sum_i h_i \sigma_i^x$, with the latter being implemented via a two-photon Raman transition [Fig. 4(a)]. In the high frequency limit, the dynamics are governed by an effective Hamiltonian:
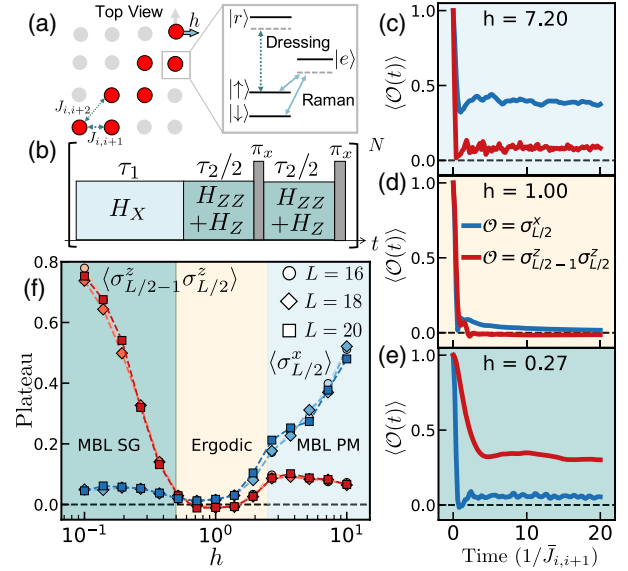

FIG. 4. (a) Schematic of the proposed experimental protocol. Within an optical lattice, neutral atoms are prepared along two adjacent diagonals (say, with a gas microscope), defining a zig-zag spin chain configuration. Dressing with a Rydberg state $|r\rangle$ leads to H_{ZZ} with an additional on-site field $H_Z \propto \sum_i \sigma_i^z$, while a two-photon Raman transition mediated by an excited state $|e\rangle$ leads to H_X. (b) By combining rapid spin echo pulses with Floquet evolution under H_X and $H_{ZZ} + H_Z$, one can engineer H_{eff} [Eq. (4)]. (c)–(e) Dynamics of $\sigma_{L/2}^x$ (blue) and $\sigma_{L/2-1}^z \sigma_{L/2}^z$ (red) under H_{eff} starting with initial states $|\psi_x\rangle$ and $|\psi_{zz}\rangle$, respectively. Different panels correspond to representative behaviors for the three distinct phases (tuned via h). (f) The height of the late-time plateau distinguishes between the three phases. Each data point corresponds to averaging over at least 10^2 disorder realizations.

$$H_{\text{eff}} = \frac{\tau_1}{\tau_1 + \tau_2} \sum_i h_i \sigma_i^x + \frac{\tau_2}{\tau_1 + \tau_2} \sum_{ij} J_{ij} \sigma_i^z \sigma_j^z, \quad (4)$$

where H_X is applied for time τ_1, H_{ZZ} is applied for time τ_2, and the Floquet frequency $\omega = 2\pi/(\tau_1 + \tau_2) \gg h_i$, J_{ij}. This latter inequality ensures that both Floquet heating and higher-order corrections to H_{eff} can be safely neglected on experimentally relevant timescales [45,69,70]. Note that unlike the DTC model [Eq. (3)], here Floquet engineering is being used to emulate a static MBL PM-SG Hamiltonian [71,72].

A few remarks are in order. First, by applying the Rydberg dressing to only one of the two hyperfine states [Fig. 4(a)], an additional longitudinal field $H_Z \propto \sigma_i^z$ is naturally generated. To restore the $\mathbb{Z}_2$ symmetry, one can exactly cancel this field by embedding a spin echo into the Floquet sequence [Fig. 4(b)]. In addition, varying the spacing between the echo π pulses [Fig. 4(b)] directly controls the degree of cancellation, enabling one to experimentally probe the effect of an explicit symmetry breaking field. Second, although our prior analysis has focused on eigenstate properties, these are inaccessible to

experiment. Fortunately, as we will demonstrate, the phase diagram can also be characterized via the dynamics of local observables. The intuition behind this is simple: Observables that overlap with an ℓ-bit exhibit a plateau at late times. To investigate this behavior, we use Krylov subspace methods [73–76] to numerically simulate the dynamics of H_{eff} with $\tau_1 = \tau_2 = 1$, $J_{i,i+1} \in [-1, -3]$, $J_{i,i+2} = 0.6J_{i,i+1}$ and $h_i \in [h, 3h]$. We note that the ratio of the nearest- to next-nearest-neighbor coupling strength is chosen based upon the experimentally measured Rydberg-dressing-interaction profile and a 1D zig-zag chain geometry [Fig. 4(a)] [38,77,78].

For system sizes up to $L = 20$, we compute the dynamics of initial states $|\psi_x\rangle$ and $|\psi_{zz}\rangle$ [79]; both states are easily preparable in experiment, close to zero energy density, and chosen such that $\langle \psi_x | \sigma_{L/2}^x | \psi_x \rangle = 1$ and $\langle \psi_{zz} | \sigma_{L/2-1}^z \sigma_{L/2}^z | \psi_{zz} \rangle = 1$. Starting with $|\psi_x\rangle$ as our initial state and large h, we observe that $\langle \sigma_{L/2}^x(t) \rangle$ plateaus to a finite value at late times, indicating the system is in the MBL PM phase [Fig. 4(c)]. Analogously, for $|\psi_{zz}\rangle$ and small h, we observe that $\langle \sigma_{L/2-1}^z(t) \sigma_{L/2}^z(t) \rangle$ plateaus to a finite value at late times, indicating the system is in the MBL SG phase [Fig. 4(e)]. For $h \sim 1$, *both* observables decay to zero, indicating the system is in the ergodic phase [Fig. 4(d)]. The plateau value of the two observables as a function of h clearly identifies the intervening ergodic region [Fig. 4(f)].

To ensure that one can observe the intervening ergodic phase within experimental coherence times, we now estimate the timescales necessary to carry out our protocol. Previous experiments using Rydberg dressing have demonstrated coherence times $T_2 \sim 1$ ms, with nearest neighbor couplings $J_{i,i+1} \sim (2\pi) \times 13$ kHz and a microwave-induced π-pulse duration ~ 25 μs [38]. Taken together, this leads to an estimate of ~ 55 μs for the Floquet period [Fig. 4(b)]. Crucially, within T_2 (i.e., ~ 20 Floquet cycles), all observables approach their late-time plateaus [45].

Analytic discussion.—We conclude by discussing previous analytical results and how they may shed light on the origins of the intervening ergodic phase. In the absence of interactions, the transitions we consider all fall into infinite-randomness universality classes characterized by both a divergent single-particle density of states (DOS, $D(\varepsilon) \sim |\varepsilon \log^3 \varepsilon|^{-1}$ near zero single-particle energy ε) and single-particle orbitals with diverging mean and typical localization lengths ($\xi_{\text{mean}} \sim |\log^2 \varepsilon|$ and $\xi_{\text{typ}} \sim |\log \varepsilon|$, respectively) [80–85]. These divergences suggest that two-body resonances might directly destabilize MBL upon the introduction of interactions; however, a simple counting of resonances in typical blocks does not produce such an instability: In a block of length l, there are $lN(\varepsilon)$ "active" single particle orbitals with $\xi_{\text{typ}}(\varepsilon) \geq l$, where $N(\varepsilon) = \int^\varepsilon d\varepsilon' D(\varepsilon')$ is the integrated DOS [33,45,86]. These orbitals overlap in real space and are thus susceptible to participating in perturbative two-body resonances. A perturbative instability of the

localized state arises if lN diverges as $\varepsilon \to 0$; even for arbitrarily small interactions, a large network of resonant pairs can be found at low enough energy. Using the DOS and localization lengths of the infinite-randomness transition, we find $lN \sim 1/|\log \varepsilon|$ which vanishes slowly as $\varepsilon \to 0$.

Alternatively, one might consider the susceptibility to avalanches due to rare thermal bubbles induced by the interactions [34,87,88]. For a system with a distribution of localization lengths, it has recently been shown that the *average* localization length controls this instability [35]: for $\bar{\xi} > 2/\log 2$, thermal bubbles avalanche. However, this is within a model where the orbitals have a single localization center. Near the infinite-randomness transition, the orbitals have two centers whose separation is controlled by ξ_{mean} but whose overlap onto a putative thermal bubble is controlled by ξ_{typ}. Thus, while $\overline{\xi_{\text{mean}}}$ diverges logarithmically, the more appropriate $\overline{\xi_{\text{typ}}}$ remains finite and this criterion does not produce an absolute instability [45]. We highlight that it is only a logarithmic correction which causes the convergence of the average localization length; unaccounted channels might provide an additional logarithm leading to an absolute avalanche instability. We leave this to future work.

Finally, let us note that the direct numerical observation of avalanche instabilities remains extremely challenging [34,89]; the presence of a robust intervening ergodic region in our study suggests that an alternate mechanism might be at the heart of our observations.

Note added.—Recently, we became aware of complementary work on the presence of intervening thermal phases between MBL transitions [91].

---

*These authors have contributed equally to this manuscript.
[1] I. V. Gornyi, A. D. Mirlin, and D. G. Polyakov, Phys. Rev. Lett. **95**, 206603 (2005).

[2] D. Basko, I. Aleiner, and B. Altshuler, Ann. Phys. (Amsterdam) 321, 1126 (2006).

[3] D. M. Basko, I. L. Aleiner, and B. L. Altshuler, arXiv:cond-mat/0602510.

[4] R. Nandkishore and D. A. Huse, Annu. Rev. Condens. Matter Phys. 6, 15 (2015).

[5] R. Vosk, D. A. Huse, and E. Altman, Phys. Rev. X 5, 031032 (2015).

[6] D. A. Abanin, E. Altman, I. Bloch, and M. Serbyn, Rev. Mod. Phys. 91, 021001 (2019).

[7] J. M. Deutsch, Phys. Rev. A 43, 2046 (1991).

[8] M. Srednicki, Phys. Rev. E 50, 888 (1994).

[9] E. Canovi, D. Rossini, R. Fazio, G. E. Santoro, and A. Silva, Phys. Rev. B 83, 094431 (2011).

[10] J. Eisert, M. Friesdorf, and C. Gogolin, Nat. Phys. 11, 124 (2015).

[11] M. Serbyn, Z. Papić, and D. A. Abanin, Phys. Rev. Lett. 111, 127201 (2013).

[12] B. Bauer and C. Nayak, J. Stat. Mech. (2013) P09005.

[13] D. A. Huse, R. Nandkishore, V. Oganesyan, A. Pal, and S. L. Sondhi, Phys. Rev. B 88, 014206 (2013).

[14] S. A. Parameswaran and R. Vasseur, Rep. Prog. Phys. 81, 082501 (2018).

[15] A. Chandran, V. Khemani, C. R. Laumann, and S. L. Sondhi, Phys. Rev. B 89, 144201 (2014).

[16] J. A. Kjäll, J. H. Bardarson, and F. Pollmann, Phys. Rev. Lett. 113, 107204 (2014).

[17] D. Pekker, G. Refael, E. Altman, E. Demler, and V. Oganesyan, Phys. Rev. X 4, 011052 (2014).

[18] Y. Bahri, R. Vosk, E. Altman, and A. Vishwanath, Nat. Commun. 6, 7341 (2015).

[19] N. Y. Yao, C. R. Laumann, and A. Vishwanath, arXiv:1508.06995.

[20] N. Y. Yao, A. C. Potter, I.-D. Potirniche, and A. Vishwanath, Phys. Rev. Lett. 118, 030401 (2017).

[21] D. V. Else, B. Bauer, and C. Nayak, Phys. Rev. Lett. 117, 090402 (2016).

[22] I.-D. Potirniche, A. C. Potter, M. Schleier-Smith, A. Vishwanath, and N. Y. Yao, Phys. Rev. Lett. 119, 123601 (2017).

[23] D. A. Huse, R. Nandkishore, and V. Oganesyan, Phys. Rev. B 90, 174202 (2014).

[24] S. Sachdev, *Quantum Phase Transitions* (Cambridge University Press, Cambridge, England, 2001).

[25] D. Pekker, G. Refael, E. Altman, E. Demler, and V. Oganesyan, Phys. Rev. X 4, 011052 (2014).

[26] J. Venderley, V. Khemani, and E.-A. Kim, Phys. Rev. Lett. 120, 257204 (2018).

[27] A. J. Friedman, R. Vasseur, A. C. Potter, and S. A. Parameswaran, Phys. Rev. B 98, 064203 (2018).

[28] R. Vasseur, A. J. Friedman, S. A. Parameswaran, and A. C. Potter, Phys. Rev. B 93, 134207 (2016).

[29] V. Khemani, A. Lazarides, R. Moessner, and S. L. Sondhi, Phys. Rev. Lett. 116, 250401 (2016).

[30] A. Chan and T. B. Wahl, J. Phys. Condens. Matter 32, 305601 (2020).

[31] T. B. Wahl and B. Béri, Phys. Rev. Research 2, 033099 (2020).

[32] B. L. Altshuler, Y. Gefen, A. Kamenev, and L. S. Levitov, Phys. Rev. Lett. 78, 2803 (1997).

[33] R. Nandkishore and A. C. Potter, Phys. Rev. B 90, 195115 (2014).

[34] W. De Roeck and F. Huveneers, Phys. Rev. B 95, 155129 (2017).

[35] P. J. D. Crowley and A. Chandran, Phys. Rev. Research 2, 033262 (2020).

[36] J. B. Balewski, A. T. Krupp, A. Gaj, S. Hofferberth, R. Lw, and T. Pfau, New J. Phys. 16, 063012 (2014).

[37] J.-y. Choi, S. Hild, J. Zeiher, P. Schauß, A. Rubio-Abadal, T. Yefsah, V. Khemani, D. A. Huse, I. Bloch, and C. Gross, Science 352, 1547 (2016).

[38] J. Zeiher, J.-y. Choi, A. Rubio-Abadal, T. Pohl, R. van Bijnen, I. Bloch, and C. Gross, Phys. Rev. X 7, 041063 (2017).

[39] H. Bernien, S. Schwartz, A. Keesling, H. Levine, A. Omran, H. Pichler, S. Choi, A. S. Zibrov, M. Endres, M. Greiner, V. Vuletić, and M. D. Lukin, Nature (London) 551, 579 (2017).

[40] A. Cooper, J. P. Covey, I. S. Madjarov, S. G. Porsev, M. S. Safronova, and M. Endres, Phys. Rev. X 8, 041055 (2018).

[41] S. d. Lsleuc, V. Lienhard, P. Scholl, D. Barredo, S. Weber, N. Lang, H. P. Bchler, T. Lahaye, and A. Browaeys, Science 365, 775 (2019).

[42] J. Wilson, S. Saskin, Y. Meng, S. Ma, R. Dilip, A. Burgers, and J. Thompson, arXiv:1912.08754.

[43] I. S. Madjarov, J. P. Covey, A. L. Shaw, J. Choi, A. Kale, A. Cooper, H. Pichler, V. Schkolnik, J. R. Williams, and M. Endres, Nat. Phys. 16, 857 (2020).

[44] We remark that up to edge effects, the model is dual under the Kramers-Wannier map ensuring that any direct transition between the MBL SG and MBL PM phases must occur at $W_J/W_h = 1$ [45].

[45] See Supplemental Material at http://link.aps.org/supplemental/10.1103/PhysRevLett.126.100604, for additional numerical simulations, characterizations of finite-size effects, methodology of the finite-size scaling analysis used to extract phase boundaries, additional information on the experimental proposal, and a more detailed discussion of the analytic arguments presented.

[46] V. Oganesyan and D. A. Huse, Phys. Rev. B 75, 155111 (2007).

[47] A. Pal and D. A. Huse, Phys. Rev. B 82, 174411 (2010).

[48] D. A. Abanin, J. H. Bardarson, G. D. Tomasi, S. Gopalakrishnan, V. Khemani, S. A. Parameswaran, F. Pollmann, A. C. Potter, M. Serbyn, and R. Vasseur, arXiv:1911.04501.

[49] D. J. Luitz, N. Laflorencie, and F. Alet, Phys. Rev. B 91, 081103(R) (2015).

[50] D. J. Luitz, Phys. Rev. B 93, 134201 (2016).

[51] R. Singh, J. H. Bardarson, and F. Pollmann, New J. Phys. 18, 023046 (2016).

[52] V. Khemani, S. P. Lim, D. N. Sheng, and D. A. Huse, Phys. Rev. X 7, 021013 (2017).

[53] P. T. Dumitrescu, R. Vasseur, and A. C. Potter, Phys. Rev. Lett. 119, 110604 (2017).

[54] F. Alet and N. Laflorencie, C. R. Phys. Quantum Simul. 19, 498 (2018).

[55] H. Theveniaut, Z. Lan, G. Meyer, and F. Alet, Phys. Rev. Research 2, 033154 (2020).

[56] D. N. Page, Phys. Rev. Lett. 71, 1291 (1993).

[57] J. M. Deutsch, Phys. Rev. A 43, 2046 (1991).

[58] M. Rigol, V. Dunjko, and M. Olshanii, Nature (London) **452,** 854 (2008).

[59] M. Srednicki, J. Phys. A **32,** 1163 (1999).

[60] A. Chandran, C. R. Laumann, and V. Oganesyan, arXiv:1509.04285.

[61] A. B. Harris, J. Phys. C **7,** 1671 (1974).

[62] R. K. Panda, A. Scardicchio, M. Schulz, S. R. Taylor, and M. Žnidarič, Europhys. Lett. **128,** 67003 (2020).

[63] Z. Papić, E. M. Stoudenmire, and D. A. Abanin, Ann. Phys. (Amsterdam) **362,** 714 (2015).

[64] We chose the form of our interaction such that, in the thermodynamic limit, the MBL SPT and MBL PM are dual to one another under the duality transformation $\sigma_i^z \to \sigma_i^z \sigma_{i+1}^x$ and $\sigma_i^x \to \sigma_{i-1}^z \sigma_i^x \sigma_{i+1}^z$.

[65] Y. Bahri and A. Vishwanath, Phys. Rev. B **89,** 155135 (2014).

[66] P. Ponte, Z. Papić, F. Huveneers, and D. A. Abanin, Phys. Rev. Lett. **114,** 140401 (2015).

[67] L. Zhang, V. Khemani, and D. A. Huse, Phys. Rev. B **94,** 224202 (2016).

[68] D. A. Abanin, W. De Roeck, and F. Huveneers, Ann. Phys. (Amsterdam) **372,** 1 (2016).

[69] D. A. Abanin, W. De Roeck, and F. Huveneers, Phys. Rev. Lett. **115,** 256803 (2015).

[70] F. Machado, G. D. Kahanamoku-Meyer, D. V. Else, C. Nayak, and N. Y. Yao, Phys. Rev. Research **1,** 033202 (2019).

[71] I.-D. Potirniche, A. C. Potter, M. Schleier-Smith, A. Vishwanath, and N. Y. Yao, Phys. Rev. Lett. **119,** 123601 (2017).

[72] J. Choi, H. Zhou, H. S. Knowles, R. Landig, S. Choi, and M. D. Lukin, Phys. Rev. X **10,** 031002 (2020).

[73] For more information, see https://zenodo.org/record/3606826.

[74] V. Hernandez, J. E. Roman, and V. Vidal, ACM Trans. Math. Softw. **31,** 351 (2005).

[75] V. Hernandez, J. E. Roman, and V. Vidal, Lect. Notes Comput. Sci. **2565,** 377 (2003).

[76] S. Balay, W. D. Gropp, L. C. McInnes, and B. F. Smith, Efficient management of parallelism in object-oriented numerical software libraries, in *Modern Software Tools for Scientific Computing*, edited by E. Arge, A. M. Bruaset, and H. P. Langtangen (Birkhäuser Boston, Boston, MA, 1997), pp. 163–202.

[77] C. Gross and I. Bloch, Science **357,** 995 (2017).

[78] An analogous behavior can be found in a linear geometry where the ratio between nearest and next-nearest neighbor interactions is $J_{i,i+2} = 0.2J_{i,i+1}$ [45].

[79] $|\psi_x\rangle$ is polarized along $+\hat{y}$ except at sites $L/2, L/2 + 1$ where it is polarized in the $+\hat{x}$ and $-\hat{x}$ direction, respectively. Analogously $|\psi_{zz}\rangle$ is polarized along $+\hat{y}$ except at sites $L/2 - 1$ through $L/2 + 2$ where the spins are polarized in the $\hat{z}$ direction with the pattern $\uparrow\uparrow\downarrow\downarrow$.

[80] F. Evers and A. D. Mirlin, Rev. Mod. Phys. **80,** 1355 (2008).

[81] D. S. Fisher, Phys. Rev. B **51,** 6411 (1995).

[82] L. Balents and M. P. A. Fisher, Phys. Rev. B **56,** 12970 (1997).

[83] B. M. McCoy and T. T. Wu, Phys. Rev. **176,** 631 (1968).

[84] Nivedita, H. Shackleton, and S. Sachdev, Phys. Rev. E **101,** 042136 (2020).

[85] Y. Kuno, T. Orito, and I. Ichinose, New J. Phys. **22,** 013032 (2020).

[86] N. Y. Yao, C. R. Laumann, S. Gopalakrishnan, M. Knap, M. Müller, E. A. Demler, and M. D. Lukin, Phys. Rev. Lett. **113,** 243002 (2014).

[87] D. J. Luitz, F. Huveneers, and W. De Roeck, Phys. Rev. Lett. **119,** 150602 (2017).

[88] T. Thiery, F. Huveneers, M. Müller, and W. De Roeck, Phys. Rev. Lett. **121,** 140601 (2018).

[89] I.-D. Potirniche, S. Banerjee, and E. Altman, Phys. Rev. B **99,** 205149 (2019).

[90] https://doi.org/10.5281/zenodo.3606826.

[91] S. Moudgalya, D. A. Huse, and V. Khemani, arXiv:2008.09113.